High Performance Nb/TiNi Nanocomposites Produced by Packaged Accumulative Roll Bonding

Daqiang Jiang[a, *], Jian Song[a], Hong Yang[b, *], Yinong Liu[b], Xiaohua Jiang[a], Yang Ren[c], Kaiyuan Yu[a], Lishan Cui[a, d, *]

[a] State Key Laboratory of Heavy Oil Processing and Department of Materials Science and Engineering, China University of Petroleum, Beijing 102249, China.

[b] Department of Mechanical Engineering, The University of Western Australia, Perth, WA 6009, Australia

[c] X-ray Science Division, Argonne National Laboratory, Argonne, IL 60439, USA

[d] Beijing Key Laboratory of Failure, Corrosion, and Protection of Oil/Gas Facilities, China University of Petroleum Beijing, Beijing 102249, China

*Corresponding author: Tel.: +86 10 89739341; fax: +86 10 89731959;

E-mail: dq80jiang@126.com, hong.yang@uwa.edu.au, lscui@cup.edu.cn

Taking full advantage of intrinsic high strength of nano-reinforcements has been proven difficult in a composite until the concept of strain matching was experimental verified in a nanowire Nb/TiNi in-situ composite, which was obtained via solidifying eutectic Nb/TiNi and subsequent severe wire drawing. However, the volume fraction of the nano-reinforcement was dictated by eutectic reaction, which severely limited the

development of high-performance composites. In this paper, the martensitic transformation nanocomposites were successfully acquired with increased volume fraction and changeable morphology of the nano-reinforcement through hot packaged ARB (PARB) and subsequent wire drawing. The nano-reinforcement with lamellar configuration in the composite could exhibit a large lattice strain of ~3.8%, which demonstrated the applicability and effectiveness of the strain matching principle in nano-lamellar composite. The obtained composites show a yield strength over 2.0 GPa and a quasi-linear elastic strain as larger as ~6.5% with adjustable apparent elastic modulus from 30-50 GPa.

Key words: Packaged accumulative roll bonding, Shape memory alloy, Martensitic transformation, Strain matching, Nanocomposite

1. Introduction

Bulk materials generally exhibit only about 10% of their possible theoretical capabilities for strength. At the meantime, nano-dimensioned materials have been found to show high strengths and elastic lattice strains approaching these theoretical limits [1-4]. Therefore, using nano-dimensioned materials, e.g. nanowires and nanofibers, as reinforcements to create super strong bulk composites has become a goal of many scientists in the recent decades. However, practice has proven challenging to harness the extraordinary properties of nanomaterials in bulk composites and these nanomaterial-reinforced bulk composites have all failed to deliver the expected promises [5]. To overcome this challenge, a new concept of “strain matching” was proposed by Hao et al. several years ago [6] by using a martensitic transformation matrix

to support the nano-reinforcement in a composite. By this concept, the martensitic transformation in the matrix provides a unique environment of uniform crystallographic lattice distortion of several percent at the atomic scale, which matches perfectly with the uniform elastic lattice strains of the nano-reinforcement, thus to induce their close to ideal strengths in the composite. Using this concept, they designed a nanowire Nb/TiNi composite by a pseudo-eutectic solidification between TiNi and Nb and subsequent in-situ conversion of the eutectic Nb into nanowires via severe wire drawing. In that composite, the Nb nanowires achieved ultra-large elastic lattice strains of 6.7%, corresponding to a strength of ~7 GPa [6].

That work, and the new “strain matching” concept, signifies a breakthrough in overcoming the long-standing challenge in nanocomposite design [7]. However, the material fabrication method of *in-situ* nanowire conversion after pseudo-eutectic solidification imposes serious limitations to the composite design. Firstly, the nano-reinforcement needs to have the ability to form a pseudo-eutectic with TiNi. This drastically restricts the number of possible candidate materials. Secondly, the volume fraction of the nano-reinforcement is dictated by the pseudo-eutectic to only about 25% volume fraction of Nb and thus cannot be increased. This limits the ultimate strength that can be achieved by the composites. Therefore, it is obvious that *ex-situ* fabrication methods, which may offer the option to alter and control the constituent volume fractions and morphologies of the composite.

Accumulative roll bonding (ARB) is the most effective method for producing bulk nanocomposites. Traditional cold ARB has been used to fabricate Mg, Al and their alloys

[8-12] with the thickness reduction of 50% in a single rolling pass thanks to their low work hardening rate, ensuring the metallurgical bonding of the stacked components and meanwhile the refinement of microstructure. However, there has not been any successful report on obtaining TiNi shape memory alloy (SMA) composite by cold ARB to date, because of strong work hardening effect of SMA. Therefore, in this paper the hot packaged ARB (PARB) was explored to fabricate martensitic transformation nanocomposite with the volume fraction and morphology of the nano-reinforcements being controllable.

2. Experimental procedure

2.1 Materials and manufacturing

Commercial TiNi sheets and Nb sheets were used in this study. Small sheets of 50 × 100 mm^2 in size were first cleaned to remove any surface contamination and then alternately stacked and packed in a steel sheath constructed of 3.5 mm thick sheets. The package was then evacuated and sealed before hot rolling at ~800 °C to bond the laminates. The diameter of the rollers was 350 mm and the rolling speed was 30 rpm. For each rolling pass the thickness reduction was ~ 90%. After that, the package was cut open and the bonded laminate composite was cut into several pieces. The pieces were cleaned and stacked in a new steel sheath and hot rolled again at 800 °C for a second pass. The procedure was repeated four times to obtain the final Nb/TiNi lamellar composite in plate form of 1.0 mm in thickness. Then thin strips of 1.0 × 1.0 mm^2 in cross section were cut from the composite plate along the rolling direction by means of electrical discharge wire cutting. The strips then underwent cold wire drawing using multiple dies to progressively reduce the wires to a 0.3 mm final diameter.

Process annealing was conducted at 750 °C for 5 min. Fig. 1 shows a schematic of the fabrication process. In this study, two composite samples were prepared. One had a Nb volume fraction of 33% and the other 49%. For the former, the initial thicknesses of the TiNi sheet and Nb sheet were 0.2 mm and 0.1 mm, respectively. For the latter, both the TiNi and Nb sheets had a thickness of 0.2 mm.

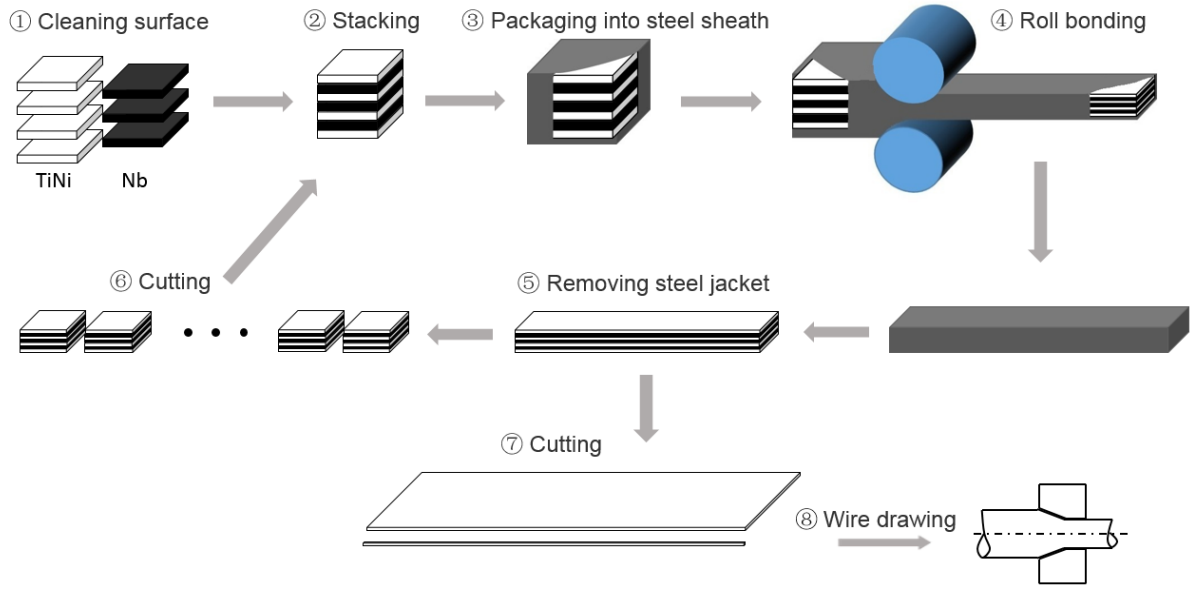

Fig. 1. Schematic diagram of the hot packaged accumulative roll bonding process and wire drawing

2.2 Testing and analysis

Quanta 200F SEM and Tecnai F20 TEM were used to observe the microstructure of the composite. In-situ synchrotron high energy X-ray diffraction (HEXRD) measurements were performed to study the deformation behavior of the constituents of the composite wires. The experiments were conducted at the 11-ID-C beamline of the Advanced Photon Source at Argonne National Laboratory, USA. High-energy X-ray with a beam size of 0.4 mm×0.4 mm and a wavelength of 0.0108 nm was used to obtain two-dimensional (2D) diffraction patterns

in the transmission geometry. Tensile testing of the composite was carried out on a WDT-II tensile testing machine with tensile strain rate of 1×10^{-3} s^{-1}. The samples used were straight wires of 70 mm in gauge length and 0.3 mm in diameter. For in-situ synchrotron measurement, shorter samples of 20 mm in length were used.

3. Results and discussion

3.1 Microstructure

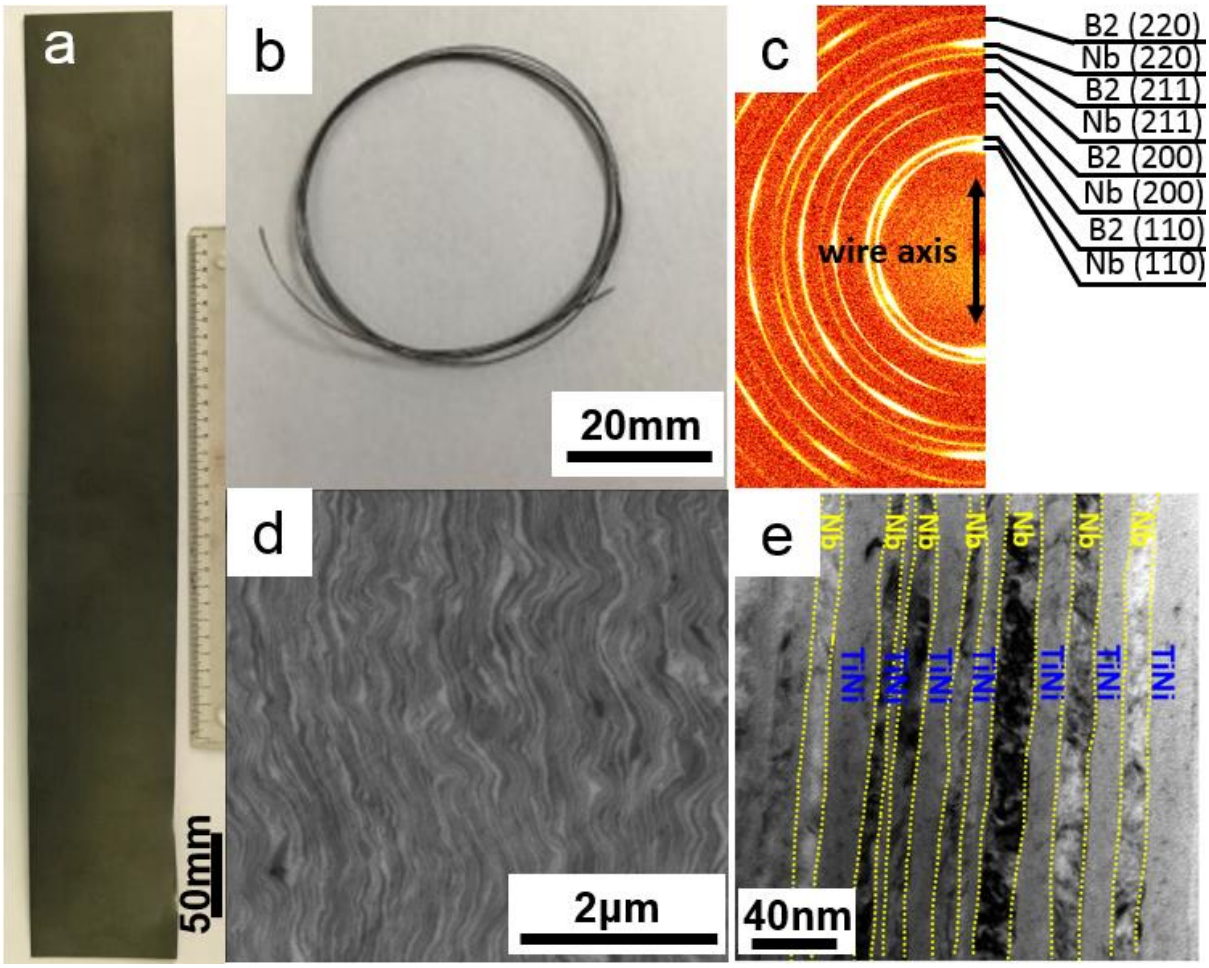

Fig. 2. Photos of multi-layered Nb/TiNi plate (a) and wire (b) with volume fraction of nano-reinforcement Nb about 49%; High energy X-ray diffraction pattern of the composite wire (c); SEM backscattered image of the cross section of the composite wire (d) (lighter

regions are the Nb layers and darker regions are the TiNi layers); TEM bright field image of the longitudinal section of the composite wire (e).

Fig. 2 shows the photos of nano-laminar composite produced with volume fraction of nano-reinforcement Nb about 49%. Fig. 2a is the composite plate produced by ARB and Fig. 2b is the composite wire formed after wire drawing. Fig. 2c is a 2-D high-energy XRD pattern of the composite wire. The pattern is fully indexed to BCC-Nb and B2-TiNi. It also reveals a strong texture of Nb <110> in the wire axial direction. Fig. 2d is an SEM backscattered electron image of the cross section of the composite wire. The lighter regions are the Nb nano-lamellae and the darker regions are TiNi layers. The cross-sectional micrographs of the Nb/TiNi multilayer composite after each roll bonding pass are presented in Fig. S1. Fig. 2e shows a TEM bright field image of the longitudinal section of the composite wire. It can be seen that the thickness of the Nb nano-lamellae was further reduced during wire drawing to ~30 nm. Detailed TEM examination revealed that the Nb - TiNi interfaces were clean and free of defects or metallurgical impurities.

3.2 Synchrotron analysis

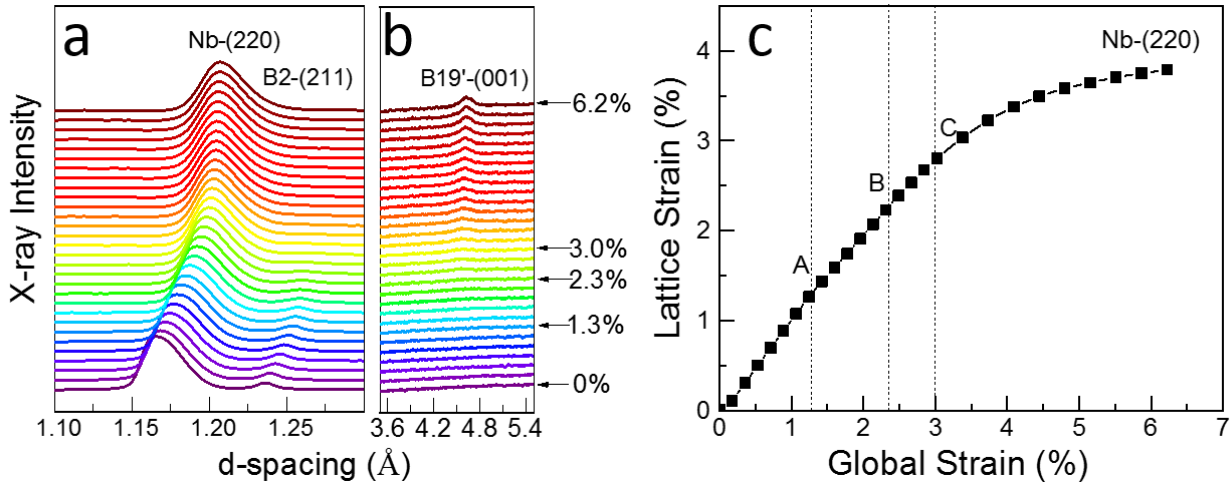

Fig. 3. Micro-deformation behavior of Nb/TiNi nano-lamellae composite (49 vol% Nb). (a) Evolution of the diffraction peaks of Nb-(220) and B2-(211) planes perpendicular to the loading direction during tensile deformation. (b) 360°-integrated HEXRD patterns showing the evolution of B19′-(001) diffraction peak during tensile deformation. (c) Evolution of the lattice strain for Nb-(220) planes in the direction perpendicular to the loading direction with the applied global strain.

High-energy synchrotron X-ray diffraction (HEXRD) was used to investigate the micro-deformation behavior of the composite during tensile deformation. The results are shown in Fig. 3. During the tensile deformation, the TiNi matrix underwent a stress-induced martensitic transformation. As seen in Fig. 3a, the intensity of the B2-(211) diffraction peaks decreased gradually with increasing the global strain. At 2.3% global strain, B19'-(001) diffraction peaks appeared as seen in Fig. 3b. The B2-(211) diffraction peak disappeared completely at 3.0% global strain. During the whole process, the Nb-(220) diffraction peaks shifted progressively to higher *d*-spacing values with increased deformation. Fig. 3c shows the *d*-spacing strains of the Nb-(220) planes calculated from the diffraction peak positions. It

reached a maximum of ~3.8%. This is ~2 times of the elastic lattice strains (~1.7%) achieved in Nb nanowires in a nanowire Nb/Cu matrix composite [13, 14]. This difference is attributed to the different mechanisms of deformation at the lattice level between the Cu matrix and the TiNi matrix. The Cu matrix deforms by dislocation slip, which has a highly heterogeneous lattice strain field. For such deformation, at the atomic scale, the local lattice strain is 100% at the site of a dislocation and typically < 0.5% away from the dislocation. Such lattice strain field is highly localized and does not match with the uniform elastic strain of 6~8% of solids (the theoretical limits). Due to this mismatch, the embedded nanomaterials in this kind of matrices are unable to be achieve ultra-large elastic strains close to the theoretical limits intrinsic to their lattices. In contrast, the TiNi matrix deforms via martensitic transformation, which is a crystallographic lattice change with a geometrical "strain" of ~7%. This crystallographic strain is uniform at the atomic (lattice) level and matches well with the theoretical limits of elastic strains of nanomaterials, both in magnitude and in atomic uniformity. This match enables effective load transfer from the TiNi matrix to the embedded nanomaterials, thus to allow them to achieve ultra-large elastic strains close to the theoretical limits. The large elastic strain achieved in this Nb/TiNi nano-lamellae composite demonstrates the applicability and effectiveness of the "lattice strain matching" principle in harnessing the intrinsic large elastic strain limit of the nano-lamellar reinforcement in the composite.

However, this elastic lattice strain of 3.8% in the Nb nano-lamellae is still much lower than what has been achieved in Nb nanowires embedded in the same TiNi matrix, as reported

earlier [6]. This is attributed to the larger aspect ratio of the nanowire form than the nanolamellar form. It has been reported that lager aspect ratio of the nano-reinforcement gives higher efficiency for load transfer from the matrix to the nano-reinforcement [15-18]. However, PARB is required to produce composites of higher volume fractions of the nano-reinforcement. Therefore, a strategy is needed to break the lamellae into discontinuous fragments and then convert them into nanowire-like by wire drawing. Earlier studies have shown that Nb nano-lamellae in the ARB Cu/Nb multilayer composite became thermal unstable at above 700 °C [19-20] and will undergo spheroidization when the thickness of the Nb layers was thinner than several tens of nanometer [21-23]. Based on this, we prolonged the annealing time before the last rolling pass since then the thickness of Nb lamellae was thin enough. Under the help of strong rolling force and long-time annealing, the Nb lamellae were fragmented. Fig. S2a and S2c shows the microstructure of cross-section and longitudinal-section of a Nb/TiNi composite plate (33 vol% Nb) after the fragmentation. It is evident that the continuous Nb lamellae had been broken and some degree of spheroidization had occurred, resulting in a structure similar to the eutectic structure of TiNi-Nb [7]. Fig. S2b and S2d shows the microstructure of cross-section and longitudinal-section of the composite wire after wire drawing. It is clear that the Nb fragments have been converted into nanoribbons. HEXRD measurement indicated that these Nb nanoribbons achieved elastic lattice strains up to 4.7% upon tensile deformation of the composite wire, as shown in Fig. S3. This demonstrated that, although the Nb was a nanoribbon not a nanowire in shape, the load transfer capability was still improved greatly due to the much larger aspect ratio of nanoribbon than nano-lamella.

3.3 Mechanical performance

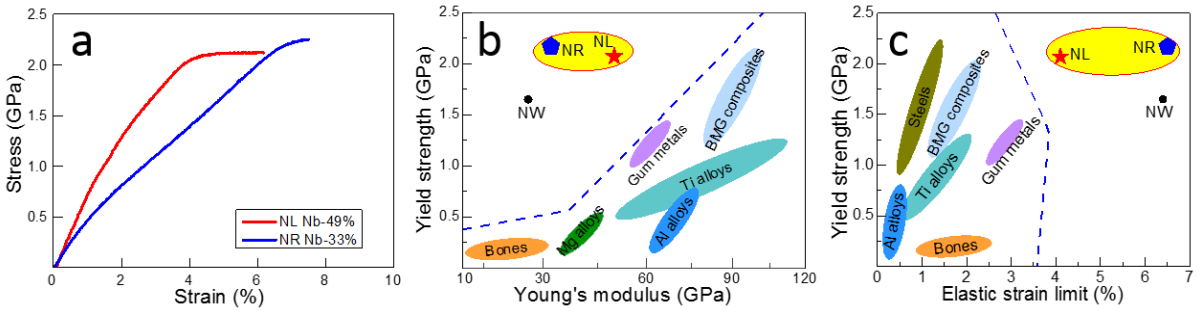

Fig. 4. Mechanical behavior of the Nb/TiNi nanocomposite. (a) Tensile stress-strain curves of the Nb/TiNi composites, the red line is for the composite of 49 vol% Nb nano-lamellae (NL) and the blue line is for the composite of 33 vol% Nb nanoribbons (NR). (b) Comparison of the yield strengths and Young's moduli of different materials. (c) Comparison of the yield strengths and elastic strain limits of different materials.

Fig. 4 shows the mechanical properties of both the nano-lamellae (NL) and the nanoribbons (NR) Nb/TiNi composite wires. It is seen that the NL composite reached a tensile yield strength of ~2.1 GPa, an elastic strain of 4.1%. The apparent elastic modulus, estimated as the average slope of the stress-strain curve up to the yield point, was measured to be 51.2 GPa. The NR composite reached a yield strength of 2.2 GPa, an elastic strain of 6.5%, and an apparent elastic modulus of ~33.8 GPa. (This sample had been pre-deformed to 8% tensile strain to encourage the coupling between the TiNi matrix and the Nb nanoribbons [6].) The "lattice strain match" enables the coupling between the large elastic strain of Nb and the transformation strain of TiNi matrix, and thus endow the composites large elastic strain. The yield strength of the NR sample is nearly 30% higher than that of the *in-situ* Nb/TiNi

nanowire (NW) sample produced from eutectic solidification [6]. This is apparently related to the 8% increase of the volume fraction of the Nb nano-reinforcement. Fig. 4b and 4c present a comparison of the mechanical properties of the Nb/TiNi nanocomposites fabricated in this study with other materials [7, 24-31]. It seen that the mechanical properties of the NL and NR Nb/TiNi composites are superior than all the reported competitor materials.

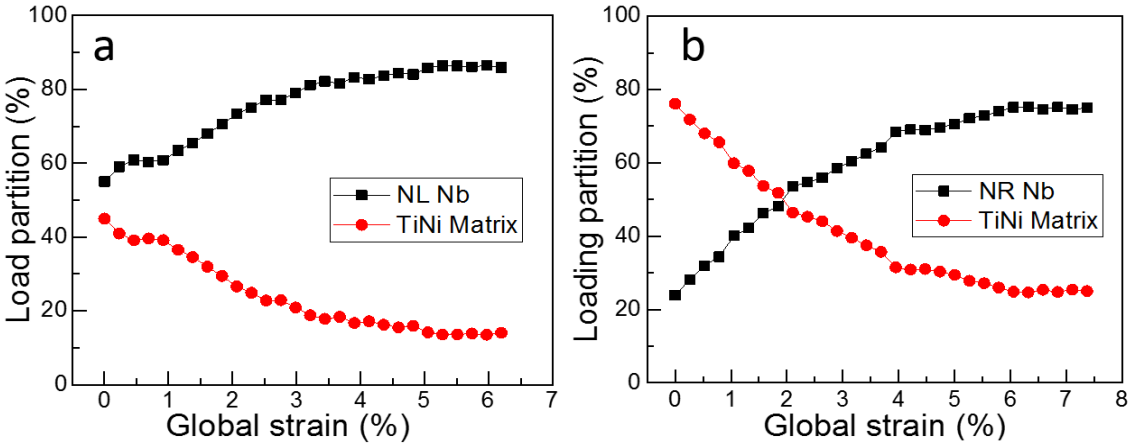

Fig. 5. Evolution of the load-sharing of the consisted components in the composites with macroscopic strain (a) 49 vol% Nb nanolamellar (NL) composites and (b) 33 vol% Nb nanoribbon (NR) composites

Based on the evolution of the elastic lattice strains of the Nb nano-reinforcement, the stress endured by the nano-reinforcement can be computed. Given its volume fraction, the external load the nano-reinforcement carried can also be estimated. Fig. 5 shows the load fractions shared by the two constituent components in the two composites. It is seen that due to higher volume fraction (49%), the Nb nanolamellae in the NL composite had a higher load sharing at the beginning of the deformation than the Nb nanoribbons in the NR composite. However, after deforming to 5% global strain, the load-sharing of the Nb nanolamellae reached 86%, by an increment of 30%. In comparison, the load-sharing of the Nb nanoribbons in the NR

composite increased from 24% to 75% after 6% of global strain, with an increment of 51%. This is apparently related to the higher elastic lattice strains achieved in the Nb nanoribbons, and demonstrates the higher efficiency of load transfer of the nanoribbon morphology compared to the nanolamellar one.

4. Conclusion

In this work, Nb/TiNi *ex-situ* nanocomposites with increased volume fraction and changeable morphology of the nano-reinforcement were successfully fabricated by PARB method. This overcomes the intrinsic volume fraction limitation of the nano-reinforcement in a composite fabricated by *in-situ* eutectic solidification method. Large elastic lattice strains were achieved in the Nb nanolamellae, demonstrating the applicability and effectiveness of the “lattice strain matching” principle. In comparison, the Nb nanoribbons exhibited a higher elastic lattice strain than the Nb nanolamellae, indicating higher internal load transfer efficiency for the Nb nanoribbon geometry than the nanolamellar geometry. The Nb/TiNi nanocomposite achieved a yield strength of 2.2 GPa and a quasi-linear elastic strain of ~6.5% with an apparent elastic modulus of ~33.8 GPa. This work demonstrates a feasible route for the preparation of martensitic transformation matrix nanocomposites with superior and adjustable mechanical properties.

Acknowledgments

These composites plates were fabricated under the help of JIYI company in Beijing, China. The authors gratefully acknowledge the financial support of the National Natural Science

Foundation of China (Grant Nos. 51571212, 51731010, 51831006, 51971243), and the financial support of Australian Research Council in grants DP180101955 and D180101744. This research used resources of the Advanced Photon Source, a U.S. Department of Energy (DOE) Office of Science User Facility operated for the DOE Office of Science by Argonne National Laboratory under Contract No. DE-AC02-06CH11357.

Conflict of Interest

The authors declare no conflict of interest

References

[1] Wong EW, Sheehan P E, Lieber CM, Nanobeam mechanics: elasticity, strength, and toughness of nanorods and nanotubes. Science 1997; 277(5334): 1971-1975.

[2] Zhu T, Li J, Ultra-strength materials. Prog Mater Sci 2010; 55(7): 710-757.

[3] Yue Y, Liu P, Zhang Z, Han X, Ma E, Approaching the theoretical elastic strain limit in copper nanowires. Nano Lett 2011; 11(8): 3151-3155.

[4] Koziol K, Vilatela J, Moisala A, Motta M, Cunniff P, Sennett M, Windle A, High-performance carbon nanotube fiber. Science 2007; 318(5858): 1892-1895.

[5] Dzenis Y, Structural nanocomposites. Science 2008; 319(5862): 419-420.

[6] Hao S, Cui L, Jiang D, Han X, Ren Y, Jiang J, Liu Y, Liu Z, Mao S, Wang Y, Li Y, Ren X, Ding X, Wang S, Yu C, Shi X, Du M, Yang F, Zheng Y, Zhang Z, Li X, Brown DE,

Li J, A transforming metal nanocomposite with large elastic strain, low modulus, and high strength. Science 2013; 339(6124): 1191-1194.

[7] Zhou M, Exceptional properties by design. Science 2013; 339(6124): 1161-1162.

[8] Ferreira F, Ferreira I, Camacho E, Lopes F, Marques AC, Velhinho A, Graphene oxide-reinforced aluminium-matrix nanostructured composites fabricated by accumulative roll bonding. Compos Part B 2019;164: 265-271.

[9] Li L, Nagai K, Yin F, Progress in cold roll bonding of metals. Sci Technol Adv Mater 2008; 9(2): 023001.

[10] Saito Y, Tsuji N, Utsunomiya H, Sakai T, Hong RG, Ultra-fine Grained Bulk Aluminum Produced by Accumulative Roll-Bonding (ARB) Process. Scr Mater 1998; 39(9): 1221-1227.

[11] Göken M, Höppel HW, Tailoring Nanostructured, Graded, and Particle-Reinforced Al Laminates by Accumulative Roll Bonding. Adv Mater 2011; 23(22-23): 2663-2668.

[12] Wu K, Chang H, Maawad E, Gan WM, Brokmeier HG, Zheng MY, Microstructure and mechanical properties of the Mg/Al laminated composite fabricated by accumulative roll bonding (ARB). Mater Sci Eng A 2010; 527(13-14): 3073-3078.

[13] Thilly L, Van Petegem S, Renault P-O, Lecouturier F, Vidal V, Schmitt B, Van Swygenhoven H, A new criterion for elasto-plastic transition in nanomaterials: Application to size and composite effects on Cu–Nb nanocomposite wires. Acta Mater 2009; 57(11): 3157-3169.

[14] Vidal V, Thilly L, Van Petegem S, Stuhr U, Lecouturier F, Renault P-O, Van Swygenhoven H, Plasticity of nanostructured Cu–Nb-based wires: Strengthening mechanisms revealed by in situ deformation under neutrons. Scr Mater 2009; 60(3): 171-174.

[15] Koo MY, Park JS, Park MK, Kim KT, Hong SH, Effect of aspect ratios of in situ formed TiB whiskers on the mechanical properties of TiBw/Ti–6Al–4V composites. Scr Mater 2012; 66(7): 487-490.

[16] Tsai J, Lu T, Investigating the load transfer efficiency in carbon nanotubes reinforced nanocomposites. Compos Struct 2009; 90(2): 172-179.

[17] Huang L, Wang L, Qian M, Zou J, High tensile-strength and ductile titanium matrix composites strengthened by TiB nanowires. Scr Mater 2017; 141: 133-137.

[18] Huang L, Qian M, Liu Z, Nguyen V, Yang L, Wang L, Zou J, In situ preparation of TiB nanowires for high-performance Ti metal matrix nanocomposites. J Alloy Comp 2018; 735: 2640-2645.

[19] Zheng S, Beyerlein IJ, Carpenter JS, Kang K, Wang J, Han W, Mara NA, High-strength and thermally stable bulk nanolayered composites due to twin-induced interfaces. Nat Commun 2013; 4: 1696.

[20] Zheng S, Carpenter JS, McCabe RJ, Beyerlein IJ, Mara NA, Engineering interface structures and thermal stabilities via SPD processing in bulk nanostructured metals. Sci Rep 2015; 4: 4226.

[21] Misra A, Hoagland RG, Effects of elevated temperature annealing on the structure and hardness of copper/niobium nanolayered films. J Mater Res 2005; 20(8): 2046-2054.

[22] Sharma G, Ramanujan RV, Tiwari GP, Instability Mechanisms in Lamellar Microstructures. Acta mater 2000; 48(4): 875-889.

[23] Carpenter JS, Zheng SJ, Zhang RF, Vogel SC, Beyerlein IJ, Mara NA, Thermal stability of Cu-Nb nanolamellar composites fabricated via accumulative roll bonding, Philos Mag 2013; 93(7): 718-735.

[24] Hofmann DC, Suh JY, Wiest A, Duan G, Lind ML, Demetriou MD, Johnson WL, Designing metallic glass matrix composites with high toughness and tensile ductility. Nature 2008; 451(7182): 1085-1089.

[25] Ashby MF, Materials selection in mechanical design, Butterworth-Heinemann, 2011.

[26] Saito T, Saito T, Furuta T, Hwang JH, Kuramoto S, Nishino K, Suzuki N, Chen R, Yamada A, Ito K, Seno Y, Nonaka T, Ikehata H, Nagasako N, Iwamoto C, Ikuhara Y, Sakuma T, Multifunctional alloys obtained via a dislocation-free plastic deformation mechanism. Science 2003; 300(5618): 464-467.

[27] Niinomi M, Recent metallic materials for biomedical applications. Metall Mater Trans A 2002; 33(3): 477-486.

[28] Niinomi M, Nakai M, Hieda J, Development of new metallic alloys for biomedical applications. Acta Biomater 2012; 8(11): 3888-3903.

[29] Jiang S, Wang H, Wu Y, Liu X, Chen H, Yao M, Gault B, Ponge D, Raabe D, Hirata A, Chen M, Wang Y, Lu Z, Ultrastrong steel via minimal lattice misfit and high-density nanoprecipitation. Nature 2017; 544(7651): 460-464.

[30] He BB, Hu B, Yen HW, Cheng GJ, Wang ZK, Luo HW, Huang MX, High dislocation density-induced large ductility in deformed and partitioned steels. Science 2017; 357(6355): 1029-1032.

[31] Liu L, Yu Q, Wang Z, Ell J, Huang MX, Ritchie RO, Making ultrastrong steel tough by grain-boundary delamination. Science 2020; 368(6497): 1347-1352.